Crystalline and magnetic anisotropy of the 3*d*-transition metal monoxides MnO, FeO, CoO, and NiO

A. Schrön,[1,2,*] C. Rödl,[1,2,3] and F. Bechstedt[1,2]

[1]*Institut für Festkörpertheorie und -optik, Friedrich-Schiller-Universität, Max-Wien-Platz 1, 07743 Jena, Germany*

[2]*European Theoretical Spectroscopy Facility (ETSF)*

[3]*Laboratoire des Solides Irradiés, Ecole Polytechnique, CEA-DSM, CNRS, 91128 Palaiseau, France*

(Received 11 July 2012; published 25 September 2012)

The magnetic-ordering and orbital-occupancy induced distortions of the rocksalt structure below the Néel temperature are computed for antiferromagnetic MnO, FeO, CoO, and NiO by means of spin-polarized density functional theory including generalized-gradient corrections and an on-site Coulomb repulsion U. The important role of the occupation of the t_{2g} minority-spin states is studied in detail for the occurring rhombohedral and monoclinic distortions. The magnetic anisotropy energy is calculated to determine the orientation of the local magnetic moments in the antiferromagnetic crystals. We take into account both the influence of spin-orbit coupling and the transverse electron interaction. The spin-orbit interaction drives the magnetic anisotropy in CoO and FeO due to the partially filled t_{2g} subshell while transverse electron interaction plays an important role for the magnetic anisotropy in MnO and NiO due to the completely empty or filled t_{2g} subshell. The results for the structural and magnetic anisotropies are discussed in the light of the available experimental data.

DOI: 10.1103/PhysRevB.86.115134 PACS number(s): 71.15.−m, 71.27.+a, 75.10.Dg, 75.30.Gw

I. INTRODUCTION

In the paramagnetic phase, the transition-metal (TM) monoxides MnO, FeO, CoO, and NiO crystallize in the rocksalt (*rs*) structure. Below their respective Néel temperatures, these oxides exhibit an antiferromagnetic ordering which is usually denoted as AFM II.[1] It can be regarded as a stacking of ferromagnetic planes with alternating direction of the local magnetic moments along the cubic [111] axis. The AFM II ordering is stabilized by superexchange which is mediated by the oxygen atoms.[2,3] In MnO and NiO the magnetic phase transition goes along with a structural distortion which reduces the symmetry of the crystal from rocksalt structure to a rhombohedral structure.[1,4–6] In the case of FeO and CoO, the rhombohedral distortion is superposed with a stronger tetragonal[1,7,8] or orthorhombic[9] distortion, which is due to an orbital-ordering induced Jahn-Teller effect and leads to a further reduction of the crystal symmetry to a monoclinic structure.[1,7–9] For FeO, however, purely rhombohedral distortions are also reported[1,10] and, thus, the actual atomic geometry is less clear than for the other transition-metal oxides (TMOs). While the structural distortions are experimentally fairly well established (aside from FeO), this is not the case for the crystallographic direction of the local magnetic moments in the antiferromagnetic phase. For MnO and NiO, measurements agree on magnetic moments lying in the (111) plane.[1,11–14] However, for FeO and CoO, various orientations have been proposed over the last decades.[1,7–10,13]

Several attempts have been made to address individual aspects of the structural distortions and to derive the orientation of the magnetic moments in the TMOs by means of *ab initio*[15,16] as well as model[17,18] calculations. In this paper we calculate both the structural distortions that accompany the magnetic phase transition and the orientation of the magnetic moments in the crystal in a consistent and systematic way from first principles for the whole series of oxides from MnO to NiO.

It has been shown (see, e.g., Refs. 19, 20, and references therein) that many structural, magnetic, and electronic properties of the TMOs can be well described within density-functional theory (DFT).[21] For instance, lattice constants and spin magnetic moments can be obtained in satisfying quantitative agreement with experiments even in the local spin-density approximation (LDA) or generalized-gradient approximation (GGA).[19,20,22,23] Other properties, such as band gaps or photoemission spectra, can only be captured qualitatively or not at all with (semi)local exchange-correlation (XC) functionals.[19] This partial failure of LDA and GGA is due to the strong localization of the TM 3*d* electrons. Various methods have been suggested to overcome the deficiencies of the local approaches: Some authors include terms that (partially) remove the self-interaction inherent in LDA/GGA.[24–26] Others use more sophisticated hybrid functionals to describe the nonlocal screened exchange.[23,27,28] However, these methods also do not predict all properties of the TMOs correctly as has been shown recently for the energetic ordering of different possible ground-state crystal structures for MnO.[29] The DFT+U approach, with U as an effective Coulomb repulsion on the d shell, is a computationally cheaper alternative to the hybrid functionals which captures the on-site interaction in an approximate way.[16,23,25,27,30,31]

In this paper we perform collinearly spin-polarized GGA+U calculations to determine the structural distortions which are due to the partial filling of the t_{2g} minority-spin subshell and the unique axis along [111] that is introduced by the magnetic ordering. The crystalline anisotropy tensor is derived subsequently from the distorted unit cells and the influence of the occupation of the t_{2g} orbitals on the tensor elements is discussed. Starting from the calculated distorted structures, we compute the total magnetic moments, that is, taking both orbital (if any) and spin contributions into account, in a noncollinear calculation including spin-orbit coupling (SOC). The magnetic anisotropy is dominated by two contributions: First, the intricate interplay of spin and

spatial degrees of freedom which is mediated by the SOC term leads to an anisotropy of the total energy of the system with respect to the spatial orientation of the local magnetic moments. The second contribution related to the interaction between the local magnetic moments becomes important only if the SOC-induced magnetic anisotropy is small or vanishes. We take both effects into account and derive the resulting orientations and magnitudes of the total magnetic moments as well as the anisotropy constants.

The computational details and applied methods are described in Sec. II. In Sec. III we discuss the structural results, while Sec. IV focuses on the magnetic anisotropy. In Sec. V a brief summary and conclusions are given.

II. COMPUTATIONAL DETAILS

All DFT calculations[21,32] have been performed using the Vienna *ab initio* simulation package (VASP).[33] The TM $3d$, TM $4s$, O $2s$, and O $2p$ electrons are considered as valence states. The one-particle wave functions are expanded in a basis set of plane waves up to a cutoff energy of 750 eV, whereas the projector-augmented-wave (PAW) method[34,35] is applied to describe the wave functions in the core regions with an accuracy comparable to all-electron calculations. The huge plane-wave cutoff is necessary to converge the total energies down to deviations smaller than 1 meV per formula unit.

The antiferromagnetically ordered TMOs are represented by rocksalt, rhombohedral, or monoclinic crystals with a (magnetic) unit cell containing four atoms. The corresponding Brillouin zones (BZ) are sampled by a mesh of $10 \times 10 \times 10$ **k** points. Also the **k**-point set is well converged to yield total energies with an accuracy of 1 meV per formula unit or better. In order to allow for spontaneous symmetry breaking due to orbital ordering, no symmetry constraints are applied during the calculations, that is, the **k**-space summations are not restricted to the irreducible part of the BZ. The internal degrees of freedom are optimized by relaxation of the shape of the unit cell as well as the atomic positions until the Hellmann-Feynman forces are below 1 meV/Å. The equilibrium volume V_0, the total energy E_{tot}, the isothermal bulk modulus B_0, and its pressure derivative B_0' are obtained by fitting the energy versus volume curves to the Murnaghan[36] equation of state.

For the description of XC in the framework of collinear spins, the GGA parametrization of Perdew, Burke, and Ernzerhof[37] (PBE) is applied. The limitations of the GGA (or LDA) for the antiferromagnetic TMOs are at least twofold: (i) It yields metallic ground states for FeO and CoO[19] and (ii) the energetic ordering of fourfold and sixfold coordinated atomic geometries is wrong for MnO.[29] Both deficiencies of the functionals can be overcome by introducing a d-d intra-atomic Coulomb energy U (and its exchange counterpart J). The present GGA+U calculations are based on the scheme of Dudarev *et al.*,[25] where only the difference between the on-site repulsion and the exchange parameter $U - J$ enters the energy functional. Therefore, all values for U given throughout this paper are effective values representing $U - J$. Many different values between $U = 0$ and 8 eV have been used in the literature to model different structural, magnetic, and electronic properties of the TMOs.[16,25,27,30,31] The value of U is set to $U = 4$ eV for all TMOs throughout this article. For instance, a localized Coulomb interaction on the d shell of this magnitude gives rise to the correct energetic ordering of crystal structures for MnO,[29] opens gaps for FeO and CoO,[28] but does not destroy the energetic ordering of the valence and conduction bands with respect to experiment and more sophisticated quasiparticle calculations.[28] Structural parameters and the magnetic moment are rather insensitive to variations of the U parameter by ± 1 eV.[29]

Relativistic effects are taken into account on two different levels as suggested by Koelling and Harmon.[38] The Darwin term and the relativistic mass correction, often referenced as the scalar-relativistic contributions, are considered already within the pseudopotential generation and are, thus, included in all calculations. Computations with spin-orbit (SO) interaction, however, need to treat noncollinear spin densities and take into account the full vector of the magnetization density.[39] Other relativistic corrections originate from transverse electron-electron interactions. They can be approximately described by magnetic dipole-dipole interactions.[40] In contrast to our approach, they are usually omitted in *ab initio* calculations of solids because of their smallness.

III. CRYSTALLINE ANISOTROPY

A. General structural, elastic, and magnetic properties

For the type-II antiferromagnetically ordered $3d$ TMOs with alternating magnetic moment directions of adjacent ferromagnetic $TM^{2+}(111)$ planes (see Fig. 1) important properties such as the atomic structure can be reasonably well described within a collinear approximation for the spin.[29] All calculations in this section are, thus, performed in the collinear framework allowing for a full relaxation of both atomic positions and unit cell shape for a given volume.

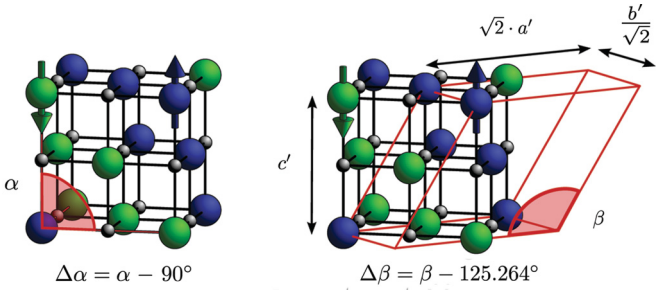

FIG. 1. (Color online) Illustration of the AFM II antiferromagnetic ordering and the lattice parameters of the TMOs. TM ions with opposite spins are indicated by large blue or green spheres while the oxygen ions are given by small gray spheres. The arrows serve as a guide to the eye to denote opposite magnetization directions and not the actual orientation of the magnetization vector in the unit cell. In the left image the pseudocubic angle α and the rhombohedral distortion angle $\Delta\alpha$ are defined. The right image shows the monoclinic unit cell together with the definitions of the monoclinic angle β, the monoclinic distortion angle $\Delta\beta$, and the pseudo-orthorhombic lattice constants a', b', and c'.

TABLE I. Computed structural, elastic, and magnetic parameters for the distorted antiferromagnetic TMOs. MnO and NiO are distorted rhombohedrally, whereas a monoclinic distortion is obtained for FeO and CoO. The rhombohedral distortion is characterized by the angular deviation $\Delta\alpha$ and the monoclinic distortion by $\Delta\beta$ as well as lattice constant ratios b'/a' and c'/a' (see Fig. 1). The computed values are compared with available experimental data. The calculated magnetic moments given here are spin magnetic moments μ_s, whereas the experimental values are total magnetic moments μ.

	MnO		FeO			CoO		NiO	
	GGA+U	Expt.	GGA+U	Expt.		GGA+U	Expt.	GGA+U	Expt.
V_0 (Å^3)	22.6	21.7–21.8[a–d]	20.9	20.0–20.3[d–f]	19.7–20.3[d,e,g–i]	19.8	19.3[d,j]	18.5	18.1–18.2[b,k]
B_0 (GPa)	143	144–159[d,l–n]	156	141–176[d,e]	141–176[d,e]	169	186[d]	186	187–238[k,o,p]
B_0'	4.3		4.5			4.4		4.4	
Distortion	$R\bar{3}m$	$R\bar{3}m$[a–c]	$C2/m$	$C2/m$[f]	$R\bar{3}m$[a,h,i]	$C2/m$	$C2/m$[a,j,q]	$R\bar{3}m$	$R\bar{3}m$[a,b,r]
$\Delta\alpha$ (deg)	0.72	0.43–0.62[a–c]	–	–	-0.45 to -0.56[h,i]	–	–	0.07	0.08–0.1[b,r]
$\Delta\beta$ (deg)	–	–	-0.48	-0.62[f]	–	0.80	0.30[j]	–	–
c'/a'	–	–	1.025	1.023[f]	–	0.976	0.988[j]	–	–
b'/a'	–	–	0.975	0.991[f]	–	0.985	0.999[j]	–	–
μ (μ_B)	4.60	4.58[b]	3.69	4.0[f]	3.3–4.6[a,i]	2.68	3.8–3.98[a,j,q]	1.62	1.9[b]

[a]Reference 1; [b]Reference 5; [c]Reference 6; [d]Reference 43; [e]Reference 44; [f]Reference 9; [g]Reference 45; [h]Reference 46; [i]Reference 10; [j]Reference 8; [k]Reference 47; [l]Reference 48; [m]Reference 49; [n]Reference 50; [o]Reference 51; [p]Reference 52; [q]Reference 7; [r]Reference 4.

In Table I the equilibrium volume V_0, the isothermal bulk modulus B_0, its pressure derivative B_0', and the local (spin) magnetic moment μ_s per TM ion are listed. In general, the computed parameters agree well with available experimental values. Of course, the volumes V_0 per cation-anion pair are slightly overestimated by 3% (or less) due to the use of the GGA. The computed inverse compressibilities B_0 are in agreement with the lowest measured values. Thereby, the clear chemical trend of decreasing volumes and increasing bulk moduli along the row MnO, FeO, CoO, and NiO is confirmed. For MnO, the spin magnetic moment μ_s agrees with the measured total magnetic moment. However, for the other three TMOs an underestimation has to be stated, in agreement with the findings of other computations within spin-polarized DFT.[20,28,41,42] This is due to the neglect of orbital contributions. The overall excellent agreement between the structural and elastic properties from our GGA+U calculations, all calculated with the same $U = 4$ eV, and the experimental results throughout the whole series of the late 3d TMOs confirms that small variations of U are of minor importance for finding structural results and spin magnetic moments in good agreement with measured data.

B. Lattice distortions and strain tensor

In the paramagnetic phase the 3d TMOs crystallize in an ideal rocksalt structure with space group $Fm\bar{3}m$ (O_h^5). However, due to the antiferromagnetic ordering AFM II and the partial occupancy of the TM 3d states distortions of the ideal rocksalt geometry occur. During the structural relaxation the symmetry of MnO and NiO is reduced to a rhombohedral structure with space group $R\bar{3}m$ (D_{3d}^5) in full agreement with experimental findings[1,4–6] and other theoretical works.[20,27,53] Goodwin *et al.*[14] also report a monoclinic distortion with $C2$ (C_2^3) symmetry for MnO, but interpret the observed distortion to be due to a "frozen-in" phonon. For FeO and CoO, the symmetry is reduced to a monoclinic structure with space group $C2/m$ (C_{2h}^3) during our calculations. Also this finding agrees well with experimental results.[1,7–9] However, for nonstoichiometric FeO also rhombohedral distortions are observed.[1,10,46]

We characterize the distortions of the ideal rocksalt geometry due to the AFM II ordering and the orbital occupancy by the rhombohedral distortion angle $\Delta\alpha$ or the monoclinic distortion angle $\Delta\beta$, and the (pseudo-)orthorhombic distortions c'/a' and b'/a', respectively. The angles $\Delta\alpha$ and $\Delta\beta$ are defined in Fig. 1 as the deviations of the distorted angle from the value of the respective angle in the ideal rs structure. Thereby, $\Delta\alpha$ is derived from the lattice parameters of a deformed face-centered cubic lattice, while $\Delta\beta$, c'/a', and b'/a' follow from the nonprimitive unit cell of a monoclinic lattice described within the ideal rs structure.

The structural distortions of the rs geometry can also be characterized by the volume-conserving monoclinic strain tensor

$$\hat{\epsilon} = \begin{pmatrix} -\frac{t}{2} & \frac{e}{2}+r & r \\ \frac{e}{2}+r & -\frac{t}{2} & r \\ r & r & t \end{pmatrix} \quad (1)$$

with $\mathrm{Tr}(\hat{\epsilon}) = 0$, which relates the distorted to the undistorted simple-cubic lattice vectors $\mathbf{a}_i' = (1+\hat{\epsilon})\,\mathbf{a}_i$, with $i = 1, 2, 3$. Three special cases may be discussed in more detail: (i) For $e = t = 0$, $\hat{\epsilon}$ describes a rhombohedral distortion in the [111] direction and the rhombohedral distortion angle $\Delta\alpha$ is given by $\Delta\alpha \approx -2r$. (ii) In the case $r = 0$, the strain tensor $\hat{\epsilon}$ describes an orthorhombic distortion with the principal axes along $x' = [110]$, $y' = [\bar{1}10]$, $z' = z = [001]$. The relative changes of the lattice constants along the principal axes are then $b'/a' \approx 1 - e$ and $c'/a' \approx 1 + (3t - e)/2$, with a', b', and c' along the principal axes. (iii) Finally, a purely tetragonal distortion along the [001] direction is obtained if $e = r = 0$. The relative change of the lattice constant along the [001] direction is then $c/a = (c'/a')_{e=0} \approx 1 + 3t/2$.

TABLE II. Computed components of the strain tensor $\hat{\epsilon}$ for the $3d$ TMOs in GGA+U with $U = 4$ eV in units of 10^{-2}. Values in parentheses have been computed in GGA, that is, $U = 0$.

	r	e	t
MnO	−0.63 (−1.44)	–	–
FeO	0.14	2.53	2.51
CoO	0.11	1.51	−1.10
NiO	−0.06 (−0.25)	–	–

The different distortions have been obtained by full relaxation fixing the volume to its equilibrium value V_0 (see Table I). The values of the components of the strain tensor $\hat{\epsilon}$ for the four TMOs are compiled in Table II, while $\Delta\alpha$, $\Delta\beta$, c'/a', and b'/a' are listed in Table I. We discuss the distortions in dependence on the gradual occupation of the minority-spin t_{2g} shell from MnO to NiO in the following.

C. Rhombohedral distortion: MnO and NiO

In the case of MnO and NiO, the components t and e of the calculated strain-tensor $\hat{\epsilon}$ vanish and, thus, a purely rhombohedral distortion along the [111] direction is obtained. The values for r listed in Table II are negative. They indicate a small reduction of the distances between the (111) planes of magnetic ions together with an increase of the atomic distances within the planes to guarantee volume conservation. The rhombohedral strain significantly decreases with the filling of the minority-spin channel t_{2g} states. For MnO the value of r obtained within GGA agrees well with that given in the literature obtained within both LDA and GGA.[20] The earliest attempt for an interpretation of this rhombohedral distortion in MnO and NiO has been made by Greenwald and Smart in terms of exchange striction.[54] The driving forces are divided into an elastic and an exchange contribution.[20] The latter part can be reasonably understood in terms of a Heisenberg model Hamiltonian.[29]

Within the GGA+U approach we find the rhombohedral distortion angle to be $\Delta\alpha = 0.72^\circ$ and $\Delta\alpha = 0.07^\circ$ for MnO and NiO, respectively. Both the direction of the distortion as well as the actual value agree excellently with experimental findings.[1,4–6] Our results also agree well with other calculations utilizing exchange and correlation by GGA+U and hybrid functionals[27] or neglecting correlation completely within older Hartree-Fock calculations.[53] The excellent agreement between experiment and GGA+U for $\Delta\alpha$ is a consequence of the better description of exchange and correlation and the use of an appropriate U parameter.

In GGA ($U = 0$ eV), on the other hand, we find $\Delta\alpha = 1.64^\circ$ and $\Delta\alpha = 0.29^\circ$ for MnO and NiO, respectively, and, thus, an overestimation of the rhombohedral distortion by roughly a factor of 2–3 for MnO or even a factor of 4 for NiO. The results found here are in full agreement with earlier LSDA/GGA calculations.[20,30] In a previous paper about the energetic ordering of various crystal structures of magnetically ordered MnO,[29] we also studied the deviations from the ideal rocksalt geometry as a function of the U parameter. We found that there is in general a strong dependence of the rhombohedral distortion on the value of U, which is most significant in the "low-U" regime with $U = 0$–2 eV, but becomes less important for higher U values. The small differences of the values presented here from the ones given in Ref. 29 are related to the change of the GGA parametrization from PW91[55,56] to PBE.[37]

D. Monoclinic distortion: FeO and CoO

In comparison to MnO and NiO the situation for FeO and CoO is more intricate. Since all components of the strain tensor (1) listed in Table II are different from zero, the symmetry of the distorted cell is monoclinic for both materials. The monoclinic distortion can be described as a superposition of a rhombohedral and an orthorhombic distortion as can be seen from the strain tensor (1). The two orthorhombic contributions e and t are an order of magnitude larger than the rhombohedral contribution r and give rise to the relative changes c'/a' and b'/a' of the lattice constants along the principal axes of the distortion. The actual values obtained for c'/a' and b'/a' after self-consistent calculation of the relaxed crystal structure are listed in Table I.

For both materials we find good agreement with experimental observations. In FeO, the unit cell is stretched by about 2.5% (GGA+U) or 2.3% (experiment, Ref. 9) along the [001] axis ($c'/a' > 1$) and compressed by about 2.5% (GGA+U) or 0.9% (experiment, Ref. 9) along the $[\bar{1}10]$ direction ($b'/a' < 1$). However, stoichiometric FeO samples are difficult to prepare experimentally; usually, $Fe_{1-x}O$ occurs together with Fe and Fe_3O_4 phases.[9,10,46] This may be the reason why other experimental results claim FeO to be rhombohedrally elongated.[1,10,46] The ratio of $c'/a' < 1$ obtained for CoO agrees qualitatively with experimental observations[1,8] and corresponds to a compression along the [001] direction of 2.4% (GGA+U) or 1.2% (experiment, Refs. 1,8). Similar to FeO, for CoO a compression along the $[\bar{1}10]$ direction is also obtained ($b'/a' < 1$) with a magnitude of 1.5%. Experimentally this contraction is observed as well, yet, with a magnitude of only 0.1%.[8] The different deviations $c'/a' > 1$ ($c'/a' < 1$) for FeO (CoO) are also apparent in the signs of the monoclinic distortion angles $\Delta\beta$ in Table I. Taking into account the sensitivity of $\Delta\beta$ with respect to the intricate interplay of all the tiny structural distortions, our values for $\Delta\beta$ are in good agreement with experimental findings.[8,9]

The orthorhombic distortion in FeO and CoO is due to the partial filling of the minority-spin t_{2g} subshell in the octahedral crystal field of the ideal rocksalt geometry. The system gains energy by reducing the symmetry and, thus, lifting the degeneracy between the empty and filled t_{2g} levels, indicating a Jahn-Teller mechanism.[57,58] In the case of FeO, the only minority-spin t_{2g} electron occupies an eigenstate given by a linear combination of TM $3d$ orbitals, $\frac{1}{\sqrt{2}}(|d_{xz}\rangle - |d_{yz}\rangle)$. In CoO, on the other hand, the two occupied electronic states are given by the linear combinations $\frac{1}{\sqrt{2}}(|d_{xz}\rangle + |d_{yz}\rangle)$ and $|d_{xy}\rangle$. The symmetry breaking induced by the occupied orbitals is clearly visible in Fig. 2, where the spin-down densities are displayed for the two monoxides. Their different shape, especially their extension in the z direction and in the xy plane, change the wave-function overlap along the orthorhombic principal axes and, hence, induce the orthorhombic distortion.

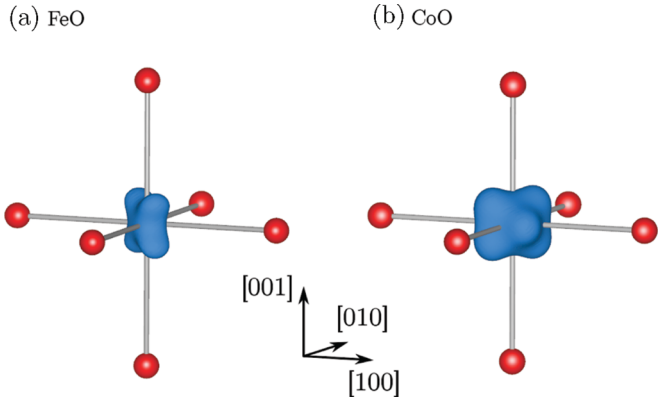

FIG. 2. (Color online) Spin density distribution for (a) FeO and (b) CoO in the magnetic unit cell. The spin densities shown here correspond to the minority-spin densities of the TM atoms and clearly show the partial occupancy of the minority-spin t_{2g} states. The red spheres indicate the positions of the oxygen ions in the distorted octahedron.

Figure 3 illustrates how the total energy of the system is minimized for the orthorhombic distortion with $c'/a' > 1$ ($c'/a' < 1$) for FeO (CoO).

E. Influence of hydrostatic pressure

There are experimental studies of TMOs (e.g. MnO) under strong hydrostatic pressure[59] which indicate several pressure-induced phase transitions between phases of different crystal structure, magnetic ordering, or even electronic structure. Here we investigate the low-pressure regime in order to understand the influence of a volume change on the structural deviations from the rs geometry. We restrict ourselves to relative volume changes smaller than 10% so that no pressure-induced phase transitions[59] or even the magnetic collapse[60] occurs. The hydrostatic pressure p associated with a volume V is calculated according to the Murnaghan equation of state

$$p = B_0/B_0'[(V_0/V)^{B_0'} - 1],$$

with V_0, B_0, and B_0' listed in Table I.

In Fig. 4 the dependence of the distortions from the ideal rs structure on the hydrostatic pressure is plotted. We discuss the rhombohedral distortion present in MnO and NiO in terms of the rhombohedral distortion angle $\Delta\alpha$ [Fig. 4(a)] and the monoclinic distortion present in FeO and CoO in terms of the monoclinic distortion angle $\Delta\beta$ and the orthorhombic distortions $c'/a' - 1$ and $b'/a' - 1$ [Fig. 4(b)]. As shown in Fig. 4(a) the application of hydrostatic pressure to MnO and NiO goes along with a considerable increase in the rhombohedral distortion, especially for MnO. In the considered pressure range the rhombohedral distortion angle $\Delta\alpha$ increases linearly with the applied pressure by a factor of 2 for both materials. This may be due to the superexchange, which is the driving force behind the rhombohedral distortion. An increase in pressure is equivalent to a decrease of the bond length and, thus, enhances the overlap between oxygen p and TM $3d$ orbitals. It leads to an increase of the *inter-atomic* exchange and, thus, of the antiferromagnetic coupling as

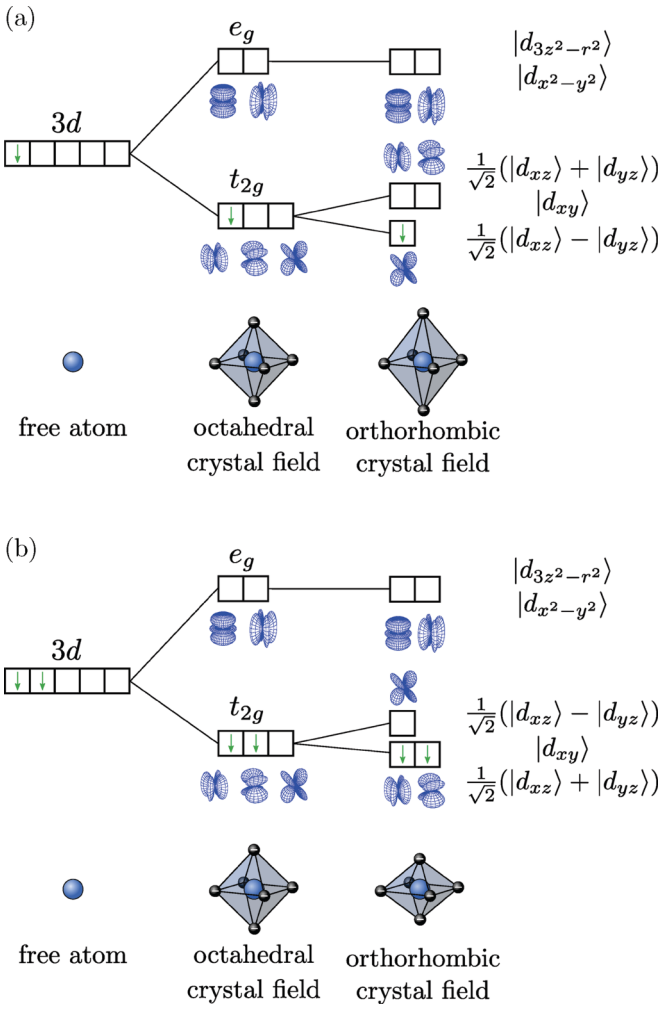

FIG. 3. (Color online) Level splittings and occupation of the $3d$ states due to the octahedral crystal field with the dominating orthorhombic distortions (schematically). Only the minority-spin channel is described. (a) Fe^{2+}, (b) Co^{2+}.

shown by studying the volume dependence of the magnetic coupling constants in Ref. 29.

For FeO and CoO the situation is different. While the application of hydrostatic pressure has almost no influence on b'/a', we find a large (small) decrease of the absolute values of c'/a' for FeO (CoO). For vanishing hydrostatic pressure we identified the dominating contribution to the monoclinic distortion to be orthorhombic with a minor rhombohedral distortion resulting in an elongation along [111] and $\Delta\beta$ to be mainly influenced by the deviation c'/a' (see Sec. III D). Consequently, the absolute value of $\Delta\beta$ decreases with increasing pressure for FeO, while it is almost constant for CoO over the whole studied pressure range. The driving force behind the distortions in FeO and CoO is the Jahn-Teller effect due to the different orbital occupancies.

Despite the strong pressure dependence of the different lattice distortions we find the local magnetic moments of the respective TM ions to be almost independent of the applied hydrostatic pressure and to vary only by a few percent in agreement with other theoretical studies.[41,61] This behavior is due to the fact that the local magnetic moments are determined

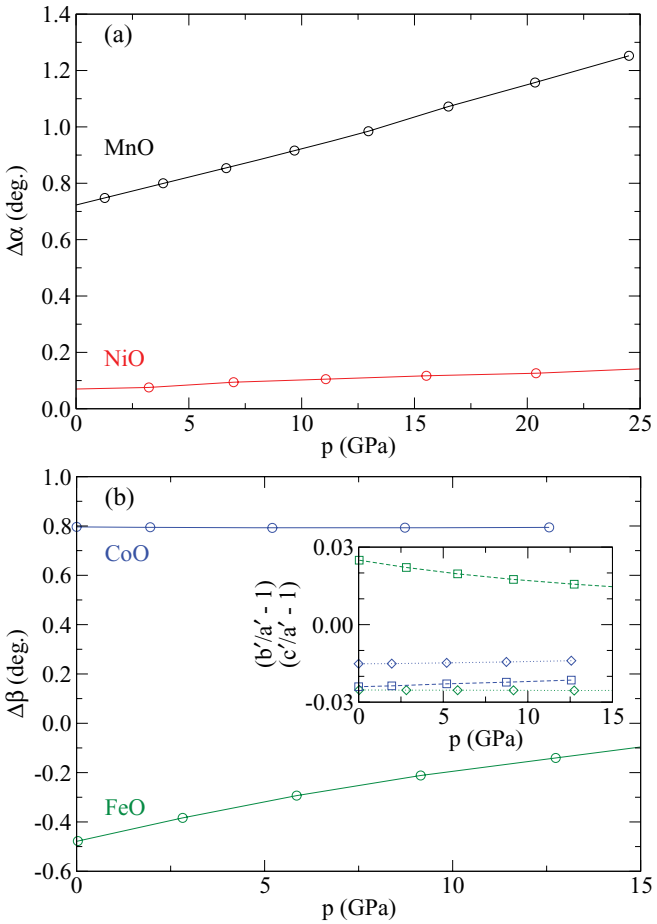

FIG. 4. (Color online) Pressure dependence of the distortion angles. (a) The rhombohedral distortion angle $\Delta\alpha$ for MnO (black solid line and circles) and NiO (red solid line and circles). (b) The monoclinic distortion angle $\Delta\beta$ (solid lines and circles), the orthorhombic distortions $b'/a' - 1$ (dotted lines and diamonds), and $c'/a' - 1$ (dashed lines and squares) are depicted for FeO (green) and CoO (blue).

mainly by *intra-atomic* exchange, which is much stronger than the *inter-atomic* interactions responsible for the lattice distortions. The *intra-atomic* exchange is, however, rather independent of the actual volume.

IV. MAGNETIC ANISOTROPY

A. General considerations

Various sources contribute to the magnetic anisotropy in crystals. The strongest influence, however, is related to the relativistic motion of the electrons in the periodic potential of the atomic cores.[62] Since the orientation of the local total angular momenta governs the magnetic anisotropy, spin has to be treated in a noncollinear approximation. A correct description of a many-body system of relativistic electrons requires the solution of a Dirac-like equation including the microscopic electromagnetic field generated by the moving electrons themselves which leads to an additional transversal electron-electron interaction beyond the "ordinary" longitudinal Coulomb interaction. In lowest nonvanishing order of v/c (v is electron velocity, and c is speed of light) the electronic retardation correction may be approximately taken into account by the Breit term.[63] Indeed, expanding the Hamiltonian up to quadratic terms v^2/c^2, one obtains a Pauli-like Hamiltonian, except from additional terms related to the Breit interaction.[64] The electric fields entering the Darwin and the spin-orbit coupling term also include contributions arising from the electron-electron Coulomb interaction, that is, Hartree and XC terms.[64] Jansen[40] has shown that a Hartree-like approximation for the current densities in the Hamiltonian including the Breit term leads to an ordinary magnetic dipole interaction term. Since relativistic corrections to XC are small, the electric field is replaced by the gradient of an effective one-electron potential including XC (i.e., in DFT the Kohn-Sham potential) in all practical computations.

Since VASP, as practically all DFT codes only includes the mass correction, the Darwin term, and the spin-orbit coupling, we study the magnetic anisotropy in a two-step procedure. In the first step we only consider spin-orbit coupling effects on the magnetic anisotropy as directly included in the code. The calculations are based on the distorted rocksalt structures obtained in Sec. III. In the second step we investigate the influence of the relativistic Breit corrections by means of a model dipole-dipole interaction term[40] using the total magnetic moments μ obtained in the first step of the procedure. Instead of the distorted rocksalt geometries obtained in Sec. III, however, we use undistorted rocksalt geometries with lattice constants leading to the same equilibrium volumes as given in Sec. III. This approximation is justified as the lattice distortions are small. While monoclinic lattice distortions only lead to small higher-order anisotropy constants beyond the ones calculated here, rhombohedral lattice distortions do not break the symmetry of the magnetic ordering AFM II and, thus, only change the magnitude of the calculated anisotropy constant slightly.

B. Spin-orbit coupling

In order to investigate the magnetic anisotropy effects arising from spin-orbit coupling, we perform fully self-consistent calculations within the GGA+U approach, but allowing for noncollinear magnetism. We use the wave functions obtained within the collinear approximation as the starting point for the subsequent noncollinear calculations. Since the entire magnetization density vector $\mathbf{m}(\mathbf{r})$ has to be computed, one expands the two spin densities $(n^{\uparrow}, n^{\downarrow})$, which are sufficient for a collinear description of the system, into a 2×2 spin-density matrix $(n^{\uparrow}, n^{\downarrow}, n^{+}, n^{-})$. This is done by an initial alignment of the two collinear spin densities $(n^{\uparrow}, n^{\downarrow})$ along a certain discretization axis $\mathbf{S}$. The off-diagonal components (n^{+}, n^{-}) of the full 2×2 spin-density matrix are initially set to zero. During the self-consistent calculation an orbital moment might be induced on the $3d$ shell along a certain direction, so that the energy gain due to the spin-orbit coupling operator is maximized. The spin-density matrix is allowed to change until a (local) minimum of the total energy is reached, possibly accompanied by a rotation of the total magnetic moment into the easy direction $\mathbf{S}_0$ away from the initial discretization axis $\mathbf{S}$.

Spin-orbit coupling stabilizes a finite orbital moment. If it is energetically favorable, a considerable on-site electron

redistribution may occur which might influence the structural distortions. However, since the lattice distortions obtained within the collinear approximation are in good agreement with experimental findings, we fix both volume and distorted crystal structure to the respective parameters in Table I. These *a priori* constraints have *a posteriori* been proven to be reasonable for all calculations, as the occurring electron redistributions are small and the calculated stress tensors deviate only slightly from uniformity.

As a consequence, the dependence of the total energy $E = E(\mathbf{S})$ on the direction $\mathbf{S}$ of the discretization axis is extremely small. In order to study this weak dependence we characterize the direction $\mathbf{S}$ by the polar angles θ and ϕ. We chose the angles such that $\theta = 0$ if $\mathbf{S}$ is parallel to the cubic [111] direction and $\phi = 0$ if $\mathbf{S}$ lies in the $(1\bar{1}0)$ plane. Then, the total energy can be divided according to

$$E(\theta,\phi) = E(0,0) + \Delta E(\theta,\phi)$$

in a large, direction-independent contribution $E(0,0)$ and a small angular-dependent variation $\Delta E(\theta,\phi)$ whose minimum with respect to θ and ϕ coincides the easy axis $\mathbf{S}_0$ of the total magnetization.

We find the angular dependence of $\Delta E(\theta,\phi)$ to vanish identically for MnO and calculate a small maximum variation $\Delta E(\theta,\phi)$ of 15 μeV for NiO. For FeO and CoO the variation of $\Delta E(\theta,\phi)$ is about two orders of magnitude stronger and the results are plotted in Fig. 5. It has been shown for systems with rhombohedral or monoclinic symmetry[62] that the anisotropy energy can be fitted to trigonometric functions according to

$$\Delta E(\theta,\phi) = \sin^2(\theta-\theta_0)\{K + K'\cos[2(\phi-\phi_0)]\}, \quad (2)$$

with the two magnetic anisotropy constants K and K'. The polar angles θ_0 and ϕ_0 define the easy axis $\mathbf{S}_0$. The easy axis $\mathbf{S}_0$ as well as the values for K and K' are listed in Table III.

Since $\Delta E(\theta,\phi)$ vanishes for MnO, no easy axis can be determined from spin-orbit interaction and, consequently, K and K' vanish as well. For FeO (CoO) we obtain an easy

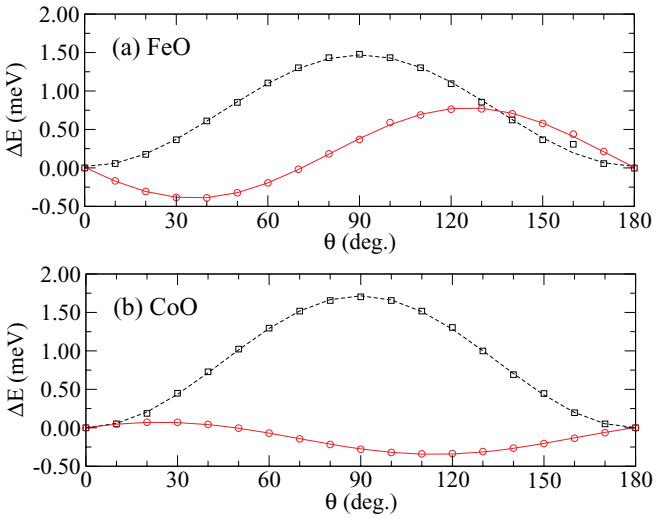

FIG. 5. (Color online) Magnetic anisotropy energy $\Delta E(\theta,\phi)$ for FeO (a) and CoO (b). Results are shown for two angles $\phi = 0^\circ$ (red circles) and $\phi = 90^\circ$ (black squares). The values obtained by *ab initio* calculations are fitted to Eq. (5) (red solid and black dashed lines).

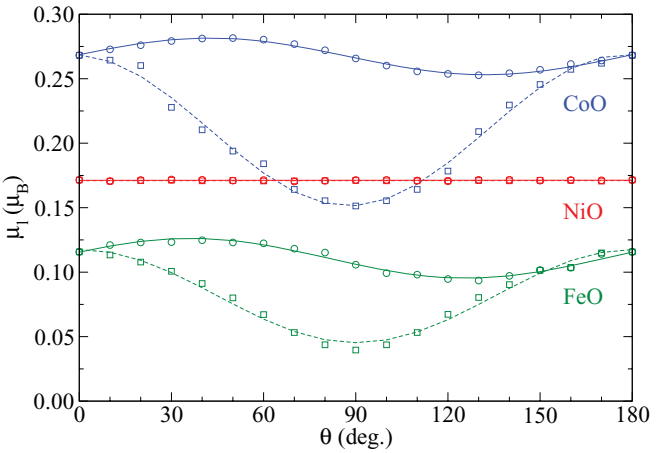

FIG. 6. (Color online) Orbital contribution $\mu_l(\theta,\phi)$ to the total magnetic moment for FeO (green), CoO (blue), and NiO (red). Circles (squares) indicate $\phi = 0^\circ$ ($\phi = 90^\circ$).

axis approximately along [110] ($[\bar{1}\bar{1}7]$) and related anisotropy constants K and K' of the order of 1 meV. For FeO experiments indicate an easy axis along or close to the [111] direction.[1,9] However, one has to keep in mind that nonstoichiometric Fe_xO samples were measured in those experiments. While the easy axis in CoO agrees well with the observations of Roth,[1] other authors propose directions different from this result.[7,8] The values of K and K' are small for NiO due to the weak variation of $\Delta E(\theta,\phi)$, but seem to indicate an easy axis along $[\bar{1}10]$ in agreement with the observations of Roth.[11] Other authors propose a possible easy axis along $[\bar{1}\bar{1}2]$.[12,13]

In order to understand the orientation of the easy directions $\mathbf{S}_0$ and the anisotropy constants K and K' obtained above, we also investigate the angular dependence of the total magnetic moments $\mu(\theta,\phi)$ and their respective spin and orbital contributions $\mu_s(\theta,\phi)$ and $\mu_l(\theta,\phi)$. The spin contribution is independent of the orientation of the discretization axis $\mathbf{S}$ for all studied TMOs. However, the orbital magnetic moment $\mu_l(\theta,\phi)$ displayed in Fig. 6 differs a lot between FeO, CoO, and NiO. The orbital moment vanishes exactly for MnO, while it is finite but almost angular independent for NiO. Consequently, for both materials the spin-orbit coupling-induced anisotropy energies $\Delta E(\theta,\phi)$ either vanish or are independent of θ and ϕ. The variation of $\mu_l(\theta,\phi)$ is much stronger in FeO and CoO and, thus, explains the significant variation of $\Delta E(\theta,\phi)$. The minimum of $\Delta E(\theta,\phi)$ coincides approximately with the maximum of $\mu_l(\theta,\phi)$ for FeO. For CoO, the minimum of $\Delta E(\theta,\phi)$ is close to the local minimum of $\mu_l(\theta,\phi)$ within the $(\bar{1}10)$ plane. Thus, we conclude that in CoO, where two electrons populate the minority-spin t_{2g} states, not only spin-orbit coupling but also exchange and correlation play an important role for the determination of the easy axis.

The absolute values of the total magnetic moments μ along the easy axis and the respective spin and orbital contributions μ_s and μ_l obtained from the noncollinear calculations are compiled in Table III. The result that the total magnetic moment in MnO is solely spin derived, $\mu = \mu_s$, is fully supported by experimentally observations.[5] The vanishing orbital contribution is due to the fact that the minority-spin channel is completely empty. For NiO we obtain a small, yet

TABLE III. Calculated easy axes, local magnetic moments, and magnetic anisotropy constants. Besides the direction of the easy axis $\mathbf{S}_0$ also its angle with the [001] direction γ is given. Furthermore, besides the norm of the total local magnetic moment (μ), the norms of the spin (μ_s) and orbital (μ_l) contributions are specified separately. The computed values are compared to experimental results.

	MnO		FeO		CoO		NiO	
	GGA+U	Expt.	GGA+U	Expt.	GGA+U	Expt.	GGA+U	Expt.
$\mathbf{S}_0$	(111)	(111)[a]	≈[110]	≈[1.0,1.8,1.4][b]	≈[−1,−1,7.2]	≈[−1,−1,7.1][a] ≈[−1,−1,3.9]/≈[110][d,e] ≈[−1,−1,2.8][g]	[$\bar{1}$10]	(111)[a,c] [$\bar{1}$10][f] [$\bar{1}\bar{1}$2][h]
γ (deg)	–	–	−90.3	−56.5[b,i]	11.1	11.3[a] ≈20/≈ −90[d,e] 27[g]	90.0	–
μ_s (μ_B)	4.60	–	3.69	–	2.68	–	1.62	–
μ_l (μ_B)	0.00	–	0.12	–	0.25	–	0.17	–
μ (μ_B)	4.60	4.58[j]	3.81	4.0[b]	2.93	3.8[a,g], 3.98[d]	1.79	1.9[j]
K (meV)	0.000	–	1.518	–	1.243	–	−0.013	–
K' (meV)	0.000	–	−0.342	–	−0.818	–	0.003	–
K_d (meV)	−0.278	–	−0.202	–	−0.126	–	−0.050	–

[a]Reference 1; [b]Reference 9; [c]Reference 65; [d]Reference 8; [e]Unclear in which direction the angle is measured; [f]Reference 66; [g]Reference 7; [h]Reference 12; [i]$\mathbf{S}_0$ not in ($1\bar{1}0$) plane; [j]Reference 5.

finite orbital moment contribution of $\mu_l \approx 0.17\ \mu_B$. Together with the spin contribution $\mu_s \approx 1.62\ \mu_B$ a total magnetic moment $\mu \approx 1.79\ \mu_B$ is obtained. This moment is in good agreement with the experimental value of $\mu \approx 1.9\ \mu_B$.[5] In contrast to MnO, the Ni minority-spin 3d shell is populated by three electrons.

The small yet finite orbital moment is a consequence of the mixing of t_{2g} and e_g states in the presence of SO coupling. In the limit of an infinitely large crystal-field splitting, this mixing would vanish and the orbital moment would be completely quenched in NiO. The crystal-field splitting between t_{2g} and e_g states, however, is of the order of ≈1 eV. Thus, the admixture of a small fraction of e_g states allows for a small orbital moment.

For FeO (CoO), an orbital moment of $\mu_l \approx 0.12\ \mu_B$ (0.25 μ_B) is obtained along the respective easy axis. The resulting total magnetic moments are $\mu \approx 3.81\ \mu_B$ (2.93 μ_B) for FeO (CoO). These values are in agreement with the results obtained by Tran *et al.*[23] within the LDA and GGA approach, but are considerably smaller than the values obtained with other XC functionals. For CoO, Solovyev *et al.*[15] found an orbital moment contribution of $\mu_l = 1\ \mu_B$ within LDA+U. Comparing with experiments, the total magnetic moment of FeO is close to the value of 4.0 μ_B measured by Fjellvåg *et al.*[9] for monoclinic FeO and lies well within the range of values obtained experimentally for rhombohedrally distorted FeO by other authors.[1,46] For CoO, the agreement with experimental results is poorer. Despite the small orbital contribution, the total magnetic moment of 2.93 μ_B is still smaller than the experimentally observed values ranging from 3.8 to 3.98.[1,7,8] In both materials, FeO and CoO, the minority-spin t_{2g} subshell is only partially occupied by one or two electrons. Thus, a maximum orbital moment of 1 μ_B is possible. However, the computed values in Table III are significantly smaller. The reason is that the level occupation depends on the energy gain due to spin-orbit coupling, whether or not it can overcome other concurring driving forces related to the longitudinal electron-electron interaction in Hartree energy and exchange and correlation. Apparently this is not the case in our GGA+U description. According to the results of Solovyev *et al.*,[15] one might argue that the gradient corrections present in a GGA+U approach in the vicinity of the Fe^{2+} and Co^{2+} ions tend to reduce the effect of the spin-orbit coupling.

C. Magnetic dipole-dipole interaction

A further relativistic correction to the total energy due to the transversal electron-electron interaction can be described by an effective magnetic dipole interaction. The corresponding energy contribution can be rewritten as a classical dipole interaction energy[40]

$$E_d = -\frac{1}{2}\frac{\mu_0}{4\pi}\iint d^3\mathbf{r}_1 d^3\mathbf{r}_2 \times \frac{3\,[\mathbf{m}(\mathbf{r}_1)\cdot\mathbf{r}_{12}]\,[\mathbf{m}(\mathbf{r}_2)\cdot\mathbf{r}_{12}] - \mathbf{m}(\mathbf{r}_1)\cdot\mathbf{m}(\mathbf{r}_2) r_{12}^2}{r_{12}^5}, \tag{3}$$

with $\mathbf{r}_{12} = \mathbf{r}_1 - \mathbf{r}_2$, $r_{12} = |\mathbf{r}_{12}|$, and the magnetization density $\mathbf{m}(\mathbf{r})$. As a second-order relativistic correction, the magnetic dipole-dipole interaction yields only a small contribution to the total energy. Therefore, we treat it in an approximate way. First, we omit the small deviations of the actual crystal structure from the ideal rs structure. Second, we replace the magnetization density around each TM atom by a local dipole with magnetic moment $\boldsymbol{\mu}_i$ located at the center $\mathbf{r}_i$ of the respective atom since the magnetization density is well localized at the TM atoms, which themselves are well separated from each other. The oxygen atoms do not contribute since their total magnetic dipole moment vanishes exactly. The local moments $\boldsymbol{\mu}_i = \mu\hat{\boldsymbol{m}}_i$ at different TM sites i possess the same absolute value μ but alternating orientations $\hat{\mathbf{m}}_i = \sigma_i\mathbf{S}$, due to the antiferromagnetic ordering. Here $\mathbf{S}$ represents a certain discretization axis and σ_i the relative orientation

(+ or −) along this axis. The total magnetic dipole-dipole interaction energy per TM atom is then approximately given by a sum over all TM sites in the crystal,

$$E_d = -\frac{1}{2}\frac{\mu_0\mu^2}{4\pi r_1^3}\sum_i \sigma_i[3\,(\mathbf{S}\cdot\hat{\mathbf{r}}_i)^2 - 1]\left(\frac{r_1}{r_i}\right)^3, \qquad (4)$$

with $r_1 = a_0/\sqrt{2}$ as the material-dependent distance between neighboring TM atoms and $\mathbf{S}\cdot\hat{\mathbf{r}}_i$ the direction cosine of the discretization axis $\mathbf{S}$ with the direction (unit) vector $\hat{\mathbf{r}}_i$ of the ith atom. While the prefactor of the sum in Eq. (4) contains the material-dependent parameters μ and r_1, the sum itself depends only on the crystal structure and the magnetic ordering.

The rocksalt crystal structure together with the antiferromagnetic ordering AFM II has rhombohedral symmetry and is, thus, uniaxial in the [111] direction. In such systems, the magnetic anisotropy contribution to the total dipole effect can be written into the form[62]

$$\Delta E_d = K_d \sin^2\theta, \qquad (5)$$

where K_d is the anisotropy constant and θ the angle of the discretization axis with the unique axis, here [111]. A positive anisotropy constant K_d corresponds to an easy axis along the unique axis, while a negative K_d leads to an easy plane perpendicular to the unique axis as illustrated in Fig. 7.

Without restricting the generality we calculate the anisotropy constant from $K_d = E_d([11\bar{2}]) - E_d([111])$, with E_d according to Eq. (4). The sum over i is independent of the TMO and contains only information about the crystal structure and the antiferromagnetic ordering AFM II. By summation over the first 1000 shells we find the sum over i in (4) to be approximately 5.113, yielding

$$K_d \approx -\frac{3}{2}\frac{\mu_0\mu^2}{4\pi r_1^3}\times 5.113$$
$$\approx -1.163\ \text{meV}\left(\frac{\mu}{\mu_B}\right)^2\left(\frac{a_0}{\text{Å}}\right)^{-3}.$$

Since K_d is always negative, the pure magnetic dipole-dipole interaction leads to an easy plane for all TMOs as depicted in Fig. 7.

The anisotropy constants listed in Table III have been computed using the total magnetic moments μ calculated in Sec. IV B and the cubic lattice constants $a_0 = 4.490$, 4.375, 4.291, and 4.200 Å of MnO, FeO, CoO, and NiO, respectively. The material dependence of the anisotropy constants is given by the factor μ^2/a_0^3. Consequently, we observe a strong decrease of the anisotropy constants K_d along the row MnO, FeO, CoO, and NiO, because of the strong decrease in the local magnetic moment due to the progressive filling of the 3d t_{2g} shell, which is not compensated by the decrease in the lattice constant a_0. The absolute magnitude of the K_d values illustrates the insignificance of the anisotropy effects due to the magnetic dipole interaction compared to the SO contribution for FeO and CoO. Thus, the resulting anisotropy energies ΔE_d are also relatively small. For that reason the magnetic dipole interaction acts as a driving force which moves the SO-induced magnetization axis somewhat towards the (111) plane for FeO and CoO.

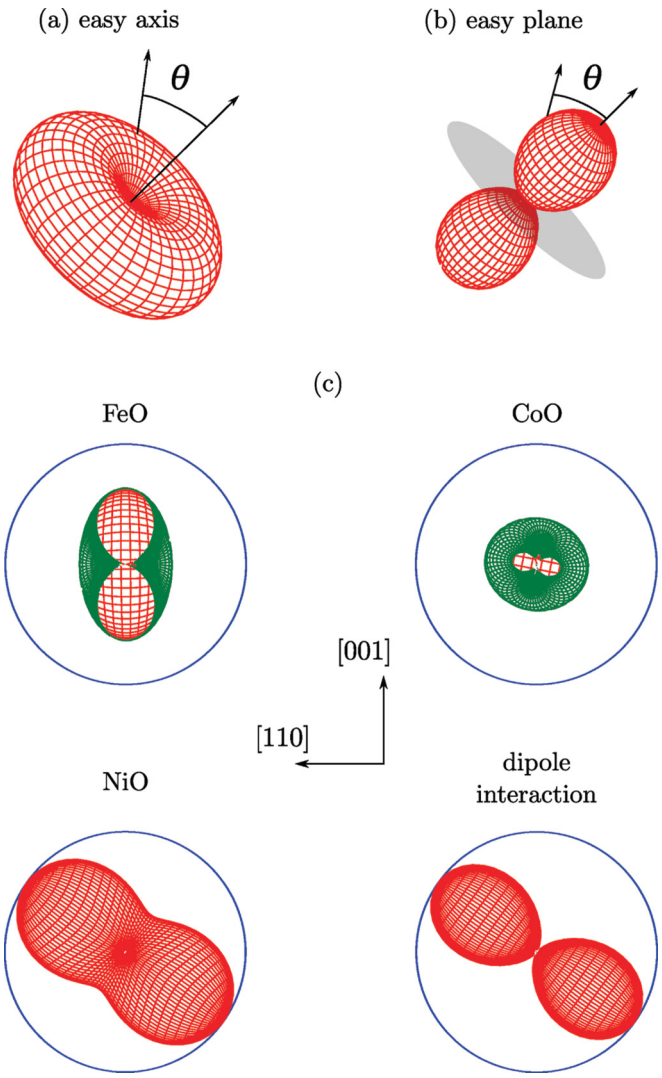

FIG. 7. (Color online) Isosurface of the magnetic anisotropy energy (5) for (a) $K_d > 0$ (yielding an easy axis) and (b) $K_d < 0$ (yielding an easy plane). (c) Visualization of the magnetic anisotropy energy obtained from SO coupling for FeO, CoO, and NiO together with the magnetic anisotropy obtained from the magnetic dipole interaction. The anisotropy of the energy $\Delta E(\theta,\phi)$ is shown in a polar plot where the distance of each point to the origin of the coordinate system indicates the magnitude of $\Delta E(\theta,\phi)$ in that direction. The blue unit spheres are normalized to the maximum anisotropy energy ($|K| + |K'| = 1$ and $|K_d| = 1$, respectively).

For NiO we find that the anisotropy constant K_d related to magnetic dipole interaction is somewhat larger than the anisotropy constants K and K' due to spin-orbit coupling. The easy axis indicated by K and K' along $[\bar{1}10]$, however, lies within the (111) plane. It is, thus, only affected by the anisotropy due to magnetic dipole interaction in the sense that any possible easy direction within the (111) plane is further stabilized with respect to an out-of-plane torsion of the magnetization vector. Finally, in MnO the magnetic dipole energy is the only contribution to the magnetic anisotropy and determines the (111) plane to be the easy plane. This

result agrees well with the fact that even experimentally only an easy plane without specification of a certain easy axis within this plane has been observed.[1,6] More recent experiments indicate, after all, a possible but weak preference of the $[\bar{1}\bar{1}2]$ direction within the (111) plane.[14] Such higher order effects can, however, not be covered by magnetic dipole interactions alone. A similar model approach has been used by Kaplan[17] and Keffer and O'Sullivan[18] based on earlier results of McKeehan[67] for the calculation of dipole magnetic anisotropy constants for MnO. They showed that higher order contributions may fix a special easy axis within the easy plane or lead to a tilting of the easy axis out of the easy plane.

V. SUMMARY AND CONCLUSIONS

We have investigated the distortions of the ideal rocksalt structure which occur in the antiferromagnetic TMOs MnO, FeO, CoO, and NiO below the Néel temperature by means of spin-polarized DFT in the GGA+U approach. The rhombohedral (MnO and NiO) or monoclinic (FeO and CoO) distortions are explained in terms of the antiferromagnetic stacking along the [111] direction and the gradual occupation of the minority-spin t_{2g} subshell from MnO to NiO. The computed distortions are not only in qualitative but also quantitative agreement with experimental findings.

The occupation of the t_{2g} levels also determines the magnetic anisotropy. In the case of MnO, the orbital moment of the minority-spin t_{2g} shell vanishes. Thus, the magnetic anisotropy arises solely from the magnetic dipole interaction and the (111) plane is the easy plane. In NiO the magnetic dipole interaction anisotropy is of the same order of magnitude as the SO-coupling induced anisotropy since the angular variation of the orbital magnetic moment is small. Both effects lead to magnetic moments lying in the (111) plane and indicate an easy direction along $[\bar{1}10]$ in agreement with experiment. In FeO and CoO the magnetic anisotropy is dominated by the strongly direction-dependent contribution of the local orbital moment. Even though an easy axis in agreement with experiment has been found for CoO, the magnitude of the orbital magnetic moment appears to be too small. In FeO, on the contrary, the magnitude of the orbital moment agrees well with measurements in contrast to the derived easy axis. The apparent underestimation of the orbital magnetic moment for CoO asks for an improved description of exchange and correlation in the energy functional.

ACKNOWLEDGMENTS

We acknowledge financial support from the European Community within the e-I3 project ETSF (GA No. 211956), the Deutsche Forschungsgemeinschaft (Project No. Be1346/20-1), and the Research Training Group (1523/1) "Quantum and Gravitational Fields" of the Friedrich-Schiller-Universität Jena. We thank Martijn Marsman from the University of Vienna for the fruitful discussions about the general theory of spin and orbital magnetism and the implementation in the VASP code.

*andreas.schroen@uni-jena.de

[1] W. L. Roth, Phys. Rev. **110**, 1333 (1958).
[2] P. W. Anderson, Phys. Rev. **79**, 350 (1950).
[3] P. W. Anderson, Solid State Phys. **14**, 99 (1963).
[4] G. A. Slack, J. Appl. Phys. **31**, 1571 (1960).
[5] A. K. Cheetham and D. A. O. Hope, Phys. Rev. B **27**, 6964 (1983).
[6] H. Shaked, J. Faber, and R. L. Hitterman, Phys. Rev. B **38**, 11901 (1988).
[7] D. Herrmann-Ronzaud, P. Burlet, and J. Rossat-Mignod, J. Phys. C **11**, 2123 (1978).
[8] W. Jauch, M. Reehuis, H. J. Bleif, F. Kubanek, and P. Pattison, Phys. Rev. B **64**, 052102 (2001).
[9] H. Fjellvåg, B. C. Hauback, T. Vogt, and S. Stølen, Am. Mineral. **87**, 347 (2002).
[10] H. Fjellvåg, F. Grønvold, S. Stølen, and B. Hauback, J. Solid State Chem. **124**, 52 (1996).
[11] W. L. Roth, Phys. Rev. **111**, 772 (1958).
[12] J. Baruchel, M. Schlenker, K. Kurosawa, and S. Saito, Philos. Mag. B **43**, 853 (1981).
[13] E. Ressouche, N. Kernavanois, L.-P. Regnault, and J.-Y. Henry, Physica B **385-386**, 394 (2006).
[14] A. L. Goodwin, M. G. Tucker, M. T. Dove, and D. A. Keen, Phys. Rev. Lett. **96**, 047209 (2006).
[15] I. V. Solovyev, A. I. Liechtenstein, and K. Terakura, Phys. Rev. Lett. **80**, 5758 (1998).
[16] A. Boussendel, N. Baadji, A. Haroun, H. Dreyssé, and M. Alouani, Phys. Rev. B **81**, 184432 (2010).
[17] J. I. Kaplan, J. Chem. Phys. **22**, 1709 (1954).
[18] F. Keffer and W. O'Sullivan, Phys. Rev. **108**, 637 (1957).
[19] K. Terakura, T. Oguchi, A. R. Williams, and J. Kübler, Phys. Rev. B **30**, 4734 (1984).
[20] J. E. Pask, D. J. Singh, I. I. Mazin, C. S. Hellberg, and J. Kortus, Phys. Rev. B **64**, 024403 (2001).
[21] P. Hohenberg and W. Kohn, Phys. Rev. **136**, B864 (1964).
[22] P. Dufek, P. Blaha, V. Sliwko, and K. Schwarz, Phys. Rev. B **49**, 10170 (1994).
[23] F. Tran, P. Blaha, K. Schwarz, and P. Novák, Phys. Rev. B **74**, 155108 (2006).
[24] V. I. Anisimov, I. V. Solovyev, M. A. Korotin, M. T. Czyzyk, and G. A. Sawatzky, Phys. Rev. B **48**, 16929 (1993).
[25] S. L. Dudarev, G. A. Botton, S. Y. Savrasov, C. J. Humphreys, and A. P. Sutton, Phys. Rev. B **57**, 1505 (1998).
[26] G. Fischer, M. Dane, A. Ernst, P. Bruno, M. Lueders, Z. Szotek, W. Temmerman, and W. Hergert, Phys. Rev. B **80**, 014408 (2009).
[27] C. Franchini, V. Bayer, R. Podloucky, J. Paier, and G. Kresse, Phys. Rev. B **72**, 045132 (2005).
[28] C. Rödl, F. Fuchs, J. Furthmüller, and F. Bechstedt, Phys. Rev. B **79**, 235114 (2009).
[29] A. Schrön, C. Rödl, and F. Bechstedt, Phys. Rev. B **82**, 165109 (2010).

[30]Z. Fang, I. V. Solovyev, H. Sawada, and K. Terakura, Phys. Rev. B **59**, 762 (1999).
[31]M. Cococcioni and S. de Gironcoli, Phys. Rev. B **71**, 035105 (2005).
[32]W. Kohn and L. J. Sham, Phys. Rev. **140**, A1133 (1965).
[33]G. Kresse and J. Furthmüller, Comput. Mater. Sci. **6**, 15 (1996).
[34]G. Kresse and D. Joubert, Phys. Rev. B **59**, 1758 (1999).
[35]P. E. Blöchl, Phys. Rev. B **50**, 17953 (1994).
[36]F. D. Murnaghan, Proc. Natl. Acad. Sci. USA **30**, 244 (1944).
[37]J. P. Perdew, K. Burke, and M. Ernzerhof, Phys. Rev. Lett. **77**, 3865 (1996).
[38]D. D. Koelling and B. N. Harmon, J. Phys. C **10**, 3107 (1977).
[39]D. Hobbs, G. Kresse, and J. Hafner, Phys. Rev. B **62**, 11556 (2000).
[40]H. J. F. Jansen, Phys. Rev. B **59**, 4699 (1999).
[41]W. Zhang, K. Koepernik, M. Richter, and H. Eschrig, Phys. Rev. B **79**, 155123 (2009).
[42]O. Bengone, M. Alouani, P. Blöchl, and J. Hugel, Phys. Rev. B **62**, 16392 (2000).
[43]Y. Sumino, M. Kumazawa, O. Nishizawa, and W. Pluschkell, J. Phys. Earth **28**, 475 (1980).
[44]J. Zhang, Phys. Rev. Lett. **84**, 507 (2000).
[45]J. Berger, F. Thomas, J. Berthon, and A. Revcolevschi, Solid State Commun. **48**, 231 (1983).
[46]P. D. Battle and A. K. Cheetham, J. Phys. C **12**, 337 (1979).
[47]Y. Noguchi, M. Uchino, H. Hikosaka, T. Atou, K. Kusaba, K. Fukuoka, T. Mashimo, and Y. Syono, J. Phys. Chem. Solids **60**, 509 (1999).
[48]S. L. Webb, I. Jackson, and J. D. F. Gerald, Phys. Earth Planet. In. **52**, 117 (1988).
[49]R. E. Pacalo and E. K. Graham, Phys. Chem. Miner. **18**, 69 (1991).
[50]J. Zhang, Phys. Chem. Miner. **26**, 644 (1999).
[51]E. Huang, High Press. Res. **13**, 307 (1995).
[52]T. Eto, S. Endo, M. Imai, Y. Katayama, and T. Kikegawa, Phys. Rev. B **61**, 14984 (2000).
[53]M. D. Towler, N. L. Allan, N. M. Harrison, V. R. Saunders, W. C. Mackrodt, and E. Aprà, Phys. Rev. B **50**, 5041 (1994).
[54]S. Greenwald and J. S. Smart, Nature (London) **166**, 523 (1950).
[55]J. P. Perdew, J. A. Chevary, S. H. Vosko, K. A. Jackson, M. R. Pederson, D. J. Singh, and C. Fiolhais, Phys. Rev. B **46**, 6671 (1992).
[56]J. P. Perdew, in *Electronic Structure of Solids '91*, edited by P. Ziesche and H. Eschrig (Akademie, Berlin, 1991), p. 11.
[57]H. A. Jahn and E. Teller, Proc. R. Soc. London Ser. A **161**, 220 (1937).
[58]H. A. Jahn, Proc. R. Soc. London Ser. A **164**, 117 (1938).
[59]C. S. Yoo, B. Maddox, J.-H. P. Klepeis, V. Iota, W. Evans, A. McMahan, M. Y. Hu, P. Chow, M. Somayazulu, D. Häusermann *et al.* , Phys. Rev. Lett. **94**, 115502 (2005).
[60]R. E. Cohen, I. I. Mazin, and D. G. Isaak, Science **275**, 654 (1997).
[61]J. Kuneš, A. V. Lukoyanov, V. I. Anisimov, R. T. Scalettar, and W. E. Pickett, Nat. Mater. **7**, 198 (2008).
[62]R. Skomski, *Simple Models of Magnetism* (Oxford University Press, Oxford, 2008).
[63]G. Breit, Phys. Rev. **34**, 553 (1929).
[64]H. A. Bethe and E. S. Salpeter, *Quantum Mechanics of One- and Two-Electron Atoms* (Academic, New York, 1957).
[65]J. R. Singer, Phys. Rev. **104**, 929 (1956).
[66]W. L. Roth and G. A. Slack, J. Appl. Phys. **31**, S352 (1960).
[67]L. W. McKeehan, Phys. Rev. **43**, 913 (1933).